Kinetic and Thermodynamic Analysis of 9-*cis*-Retinoic Acid Binding to Retinoid X Receptor α†

Michael I. Schimerlik,[‡,§] Valerie J. Peterson,[||] Peter D. Hobbs,[⊥] Marcia I. Dawson,[⊥] and Mark Leid*[,§,||]

Department of Biochemistry and Biophysics, Environmental Health Sciences Center, and Laboratory of Molecular Pharmacology, College of Pharmacy, Oregon State University, Corvallis, Oregon 97331, and Retinoid Program, SRI International, 333 Ravenswood Avenue, Menlo Park, California 94025

Received December 15, 1998; Revised Manuscript Received February 24, 1999

ABSTRACT: The interaction of retinoid X receptor α with 9-*cis*-retinoic acid was studied using stopped-flow fluorescence spectroscopy. Transient kinetic analyses of this interaction suggest a two-step binding mechanism involving a rapid, enthalpically driven pre-equilibrium followed by a slower, entropically driven reaction that may arise from a conformational change within the ligand binding domain of the receptor. The assignment of this kinetic mechanism was supported by agreement between the overall equilibrium constant, K_{ov}, derived from kinetic studies with that determined by equilibrium fluorescence titrations. Although these analyses do not preclude ligand-induced alteration in the oligomerization state of the receptor in solution, the simplest model that can be applied to these data involves the stoichiometric interaction of 9-*cis*-retinoic acid with retinoid X receptor α monomers.

Naturally occurring retinoic acids exert diverse effects on various developmental and cellular differentiation processes (*1*). These pleiotropic effects are mediated by retinoic acid (RAR)[1] and retinoid X (RXR) receptors, both of which belong to the steroid and thyroid hormone receptor superfamily of ligand-dependent transcription factors (*2*). RARs and RXRs are differentially activated by naturally occurring isomers of retinoic acid (RA): *trans*-RA, which activates only RAR family members, and 9-*cis*-retinoic acid (9cRA), which activates both classes of receptors (*3*, *4*). Members of the two families of retinoic acid receptors heterodimerize in solution and on all known RA response elements (*5*, *6*). Gene deletion studies have strongly suggested that the RXR·RAR heterodimeric complex is the functional unit of both retinoic acid signaling pathways (*7*). RA response elements are generally composed of direct repeats of the hexanucleotide sequence, AGG/TTCA, separated by 1, 2, or 5 bp (*8*). RXR·RAR heterodimeric complexes bind to RAREs with a particular orientation in which RXR occupies the 5′ half-site, whereas RAR binds to the 3′ half-site in the context of a direct repeat spaced by 2 or 5 bp (*9*−*11*). However, this polarity is reversed in the context of a direct repeat spaced by 1 bp (*11*). Although it has been previously reported that RXR was unable to bind ligand and/or activate transcription in the context of an RXR·RAR heterodimeric complex bound to RA response elements (*10*, *12*), other groups have since demonstrated the contrary (*13*−*16*). In addition, the function of the RXR ligand binding domain (LBD) appears to be regulated allosterically by the RAR LBD such that ligand binding by the RAR LBD facilitates ligand binding of and/or transcriptional activation mediated by the RXR LBD (*14*, *15*).

Ligand binding by RARs and RXRs, and possibly all ligand-activated nuclear receptors, appears to stabilize a LBD conformation that is unfavorable for interaction of the receptor with corepressor complexes and promotes interaction of the receptor with transcriptional coactivator complexes (*17*, *18*). In this way, ligand-induced conformational change functions as a molecular switch between transcriptional repression and activation. Ligand-induced conformational changes have been demonstrated for both RARs and RXRs using the techniques of differential proteolytic sensitivity (*14*, *19*, *20*) and fluorescence spectroscopy (*21*−*24*). These results are consistent with crystallographic data (*25*−*28*) which have shown that ligand binding induces (1) a large rearrangement involving LBD helices 11 and 12, (2) bending of helix 3, and (3) rotation of the omega loop separating helices 1 and 2 and 3. In the case of liganded RARγ, the repositioned helix 12 forms the lid of the ligand binding pocket (*25*). The ligand-induced rearrangement of helix 12 also juxtaposes the core of the ligand-dependent transcriptional activation function (AF-2), contained within helix 12, with helices 3−5 (*18*, *25*, *26*, *28*), creating an interface that is competent for interaction with transcriptional coactivators (*29*−*34*).

† This work was supported by Grant ES00040 from the National Institute of Environmental Health Sciences (M.I.S. and M.L.), Grant CA51993 from the National Cancer Institute (M.I.D. and M.L.), and Grant BIR-9512166 from the National Science Foundation (M.I.S. and M.L.). M.L. is an Established Investigator of the American Heart Association (Grant 9640219N).

* To whom correspondence should be addressed: Laboratory of Molecular Pharmacology, College of Pharmacy, Oregon State University, Corvallis, OR 97331. Telephone: (541) 737-5809. Fax: (541) 737-3999. E-mail: Mark.Leid@orst.edu.

‡ Department of Biochemistry and Biophysics, Oregon State University.

§ Environmental Health Sciences Center, Oregon State University.

|| Laboratory of Molecular Pharmacology, College of Pharmacy, Oregon State University.

⊥ SRI International.

[1] Abbreviations: RAR, retinoic acid receptor; RXR, retinoid X receptor; LBD, ligand binding domain; RA, retinoic acid; 9cRA, 9-*cis*-retinoic acid; DTT, dithiothreitol; CHAPS, 3-[(3-cholamidopropyl)-dimethylammonio]-1-propanesulfonate; CAPS, 3-(cyclohexylamino)-1-propanesulfonate; SR11246, 4-[1-(5,6,7,8-tetrahydro-5,5,8,8-tetramethyl-2-naphthalenyl)cyclopropyl]benzoic acid.

10.1021/bi9829478 CCC: $18.00
Published on Web 05/01/1999

Although a great deal is known concerning the structural detail of apo and holo retinoic acid receptors, a kinetic analysis of ligand binding by these receptors is lacking. Thus, we have utilized stopped-flow fluorescence spectroscopy and transient kinetic analyses to examine the mechanism of 9cRA binding to purified mouse RXRα. These kinetic data suggest that 9cRA interacts with RXR in a two-step binding mechanism with an overall equilibrium constant that is in good agreement with equilibrium binding data. The first step of the binding reaction appears to be enthalpically driven, whereas the second step is dominated by a large and favorable entropic change. To our knowledge, these data provide the first kinetic analyses of ligand interactions with any nuclear receptor on a millisecond time scale and should be useful in the development of a molecular framework for modeling the interaction of various agonist and antagonist ligands with nuclear receptors.

EXPERIMENTAL PROCEDURES

Plasmid Construction and Protein Purification. The construction, expression in *Escherichia coli* strain BL21 (DE3) plysS, and purification by nickel chelate chromatography of mouse RXRαΔAB-His (RXRα) were described previously (*6*, *20*).

Fluorescence Quenching Experiments. Fluorescence measurements were taken at various receptor concentrations in 3.0 mL of buffer containing 10 mM Na/Hepes (pH 7.8), 10% glycerol, 150 mM NaCl, 0.5 mM DTT, and 0.1 mM EDTA (buffer TD150). All experiments were performed on a SLM 8000C spectrofluorometer using excitation and emission slit widths of 8 nm. The excitation and emission maxima of RXRαΔAB-His were empirically determined to be 280 and 337 nm, respectively. For 9cRA binding experiments, samples were allowed to equilibrate for 1 min in the dark after addition of ligand prior to fluorescence determinations. Additions from concentrated stock solutions of 9cRA were made sequentially to a single sample, and the fluorescence emission was corrected for dilution.

Transient Kinetic Experiments. Stopped-flow experiments were carried out using a Biologic SFM-4 stopped-flow fluorometer having an estimated dead time ranging from 4.5 to 2.3 ms depending on the drive sequence that was used. The temperature was maintained using a circulating water temperature bath. Excitation was at 280 nm with a 1 mm slit width using a 150 W mercury/xenon lamp, and emission was followed using an Oriel 51125 band-pass filter. Each experiment consisted of three to seven kinetic traces with 2501 data points per trace. Data files were transferred to a Gateway 4DX2-66V computer for analysis (see below).

HPLC Analysis of RXRα. The method used for HPLC analysis of RXRα was similar to that described by Chen and co-workers (*35*). RXR preparations (4.2 μM, purified by nickel chelate chromatography) were dialyzed against 10 mM Tris-HCl (pH 7.8), 1 mM DTT, 500 mM NaCl, and 0.05% w/v CHAPS (TDN buffer; *35*) and applied to 1.6 cm × 60 cm Superdex 200 gel filtration column (Pharmacia) equilibrated in TDN buffer with or without 5 μM 9cRA. The HPLC column, eluted at 22 °C and at a rate of 0.4 mL/min, was calibrated using apoferritin (443 kDa), β-amylase (200 kDa), alcohol dehydrogenase (150 kDa), phosphorylase b (97 kDa), bovine serum albumin (66 kDa), ovalbumin (45 kDa), and carbonic anhydrase (31 kDa, Sigma). Protein elution from the column was monitored by absorbance at 280 nm using an in-line detector (Beckman System Gold).

Native Gel Analysis of RXRα. The method for native gel analyses was described by Chen and colleagues (*35*) with minor modifications. Purified RXRα (5−10 μg in TD150) was incubated with vehicle (ethanol) or 10 μM 9cRA for 60 min at 0 °C and then applied to a 4 to 20% acrylamide gradient gel (5 cm × 8 cm; Bio-Rad) equilibrated in 60 mM Tris/40 mM CAPS (pH 9.6) with or without 10 μM 9cRA. Gels containing liganded RXRα were developed with 10 μM 9cRA in both top and bottom buffer reservoirs. Electrophoresis was carried at 4 °C for approximately 2 h under 10 mA constant current conditions. RXRα species and protein standards (apoferritin, phosphorylase b, and carbonic anhydrase) were visualized by Coomassie blue staining. Protein standards were used to estimate the M_r of RXRα species and to align gels run in the absence and presence of 9cRA.

Data Analysis. Stern−Volmer constants for fluorescence quenching of RXRα by acrylamide, $NaNO_3$, and KI were derived by linear regression analysis of collisional quenching data:

$$\frac{F_0}{F} = 1 + KQ \tag{1}$$

where F_0 and F represent the fluorescence emission of RXRα in the absence and presence of a chemical quencher at concentration Q, respectively, and K is the Stern−Volmer constant (*36*).

All other data were analyzed using the equation fitter Scientist (Micromath Scientific Software, Salt Lake City, UT). Results from equilibrium experiments for determining the overall dissociation constant for 9cRA binding to RXRα were analyzed by fitting the percent fluorescence quenching as a function of 9cRA concentration where the percent quench was corrected for 9cRA absorption according to Lakowicz (*36*) and for the loss of fluorescence due to photolysis of the receptor:

$$\%\ \text{fluorescence quenching} = \frac{(100)(1 - Z)(2l_0)}{(R_0 + l_0 + K_d) + \sqrt{(R_0 + l_0 + K_d)^2 - 4R_0l_0}} \tag{2}$$

In eq 2, l_0 and R_0 are the total concentrations of 9cRA and RXRα monomer, respectively, K_d is the overall dissociation constant for 9cRA binding to RXRα, and Z represents the ratio of fluorescence enhancement for the RXRα·9cRA complex divided by that for the uncomplexed receptor.

Single-exponential curves describing a decrease or increase in fluorescence as a function of time were fit to eqs 3 and 4, respectively:

$$y(t) = A_1 + A_2e^{-t/\tau} \tag{3}$$

$$y(t) = A_1 + A_2(1 - e^{-t/\tau}) + k_2t \tag{4}$$

In eq 3, which was used to analyze 9cRA binding to RXRα, $y(t)$ is the fluorescence at time t, A_1 is the fluorescence at equilibrium, and the exponential curve is characterized by an amplitude A_2 and a reciprocal relaxation time, $1/\tau$. Kinetic experiments in which the rate for dissociation of 9cRA from

RXRα by displacement with the RXR-selective agonist SR11246 was measured (*37*, *38*) were analyzed using eq 4. A slower, steady state fluorescence increase which can tentatively be attributed to photochemical reactions involving SR11246 at longer times was superimposed on the single-exponential increase describing 9cRA dissociation. In eq 4, A_1 is the fluorescence at time zero, A_2 is the amplitude of the exponential increase in fluorescence, and k_2 is the additional steady state rate of fluorescence increase.

Data describing the hyperbolic dependence of $1/\tau$ on 9cRA concentration were analyzed according to a two-step kinetic mechanism:

$$\text{RXR}\alpha + 9\text{cRA} \overset{K}{\rightleftharpoons} C_1 \overset{k_1}{\underset{k_2}{\rightleftharpoons}} C_2 \qquad (5)$$

where the formation of complex C_1 was assumed to be rapid and the fluorescence quenching was attributed to the slower kinetic step forming C_2. For this mechanism under conditions where total 9cRA (l_0) is in excess over RXRα concentration:

$$\frac{1}{\tau} = k_2 + \frac{k_1 l_0}{K + l_0} \qquad (6)$$

In the fitting procedure, k_2, which was determined independently from dissociation experiments, was constrained to calculate values for k_1 and K (eq 6).

The dependence of k_2, k_1, and K on temperature was analyzed according to either Arrhenius plots (for rate constants) or van't Hoff plots for the pre-equilibrium constant K, $K_1 = k_2/k_1$, and the overall equilibrium constant $K_{ov} = K(k_2/k_1)$.

$$\ln k = \ln A - \frac{E_a}{RT} \qquad (7)$$

$$\ln K = \frac{\Delta H^\circ}{RT} + C \qquad (8)$$

For the Arrhenius plots (eq 7), A is the pre-exponential factor, E_a is the energy of activation, R is the universal gas constant, C is a constant term ,and T is the absolute temperature (kelvin). The van't Hoff plot (eq 8) was used to calculate the values for the change in standard enthalpy, ΔH°, for either step in the reaction (K or $K_1 = k_2/k_1$) or for the overall binding reaction (K_{ov}). In fitting to eqs 7 and 8, the data were weighted by $1/\sigma^2$ where weighting factors were renormalized for the semilogarithmic fits according to Bevington (*39*).

RESULTS

In agreement with results from other laboratories (*21*, *22*, *35*), the addition of 9cRA resulted in a quenching of RXRα tryptophan fluorescence without an obvious change in the shape of the emission spectrum (data not shown). The dependence of RXRα fluorescence intensity at 337 nm on 9cRA concentration is shown in Figure 1. The fit of the data to eq 2 was consistent with a single class of binding sites having a K_D equal to 7.6 nM and a relative fluorescence enhancement for the 9cRA·RXRα complex compared to free RXRα of 0.45.

RXRα possesses two tryptophan residues, either of which may be involved in 9cRA-induced quenching of RXRα

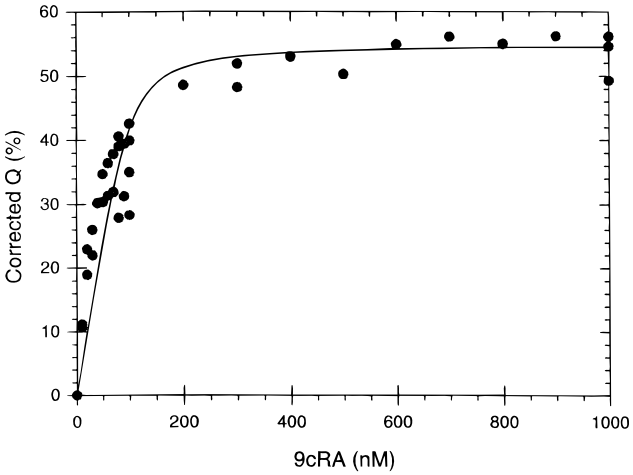

FIGURE 1: Fluorescence quenching of RXRα by 9cRA. RXRα (40 nM) was titrated with 9cRA as described in Experimental Procedures. Data from three independent experiments were fit to eq 2, giving the following parameter estimates: $K_d = 7.6 \pm 3.8$ nM and $Z = 0.45 \pm 0.02$.

fluorescence emission. Trp^{287} and Trp^{310} are located in LBD helices 3 and 5, respectively, both of which are within regions lining the ligand binding pocket and/or previously demonstrated to undergo ligand-induced conformational alterations (*25*−*27*). To address the solvent accessibility of RXRα tryptophan residues, collisional quenching experiments were conducted with three different quenchers: acrylamide, $NaNO_3$, and KI. Free tryptophan, which has a very high solvent accessibility, was used as a reference compound for all chemical quenching experiments. Linear Stern−Volmer plots were observed for all three quenchers (Figure 2A−C). Stern−Volmer constants for acrylamide and $NaNO_3$ quenching of RXRα differed by only a factor of 2 or 3 from those constants derived using free tryptophan (Figure 2A,B). However, the Stern−Volmer constant for KI quenching of RXRα fluorescence was approximately 10-fold lower than that determined for quenching of free tryptophan (Figure 2C). Whereas both acrylamide and oxygen-type quenchers, such as $NaNO_3$, partition into the hydrophobic core of proteins and effect fluorescence quenching, the large and hydrated iodide anion does so with much less efficiency (*36*). Thus, a relatively low Stern−Volmer constant for quenching of tryptophan fluorescence by KI can be diagnostic of a lack of solvent accessibility by one or both RXRα tryptophan residues. If the low Stern−Volmer constant for quenching of RXRα fluorescence by KI were due to limited solvent accessibility, the magnitude of this constant should be sensitive to the folded state of the protein. To test this hypothesis, we carried out KI quenching studies using native RXRα and receptor that was denatured with 6 M guanidine HCl. Two differences were noticed between unfolded and native RXRα. First, the emission spectra of unfolded RXRα were red shifted relative to those of the native receptor (Figure 3A). Second, the Stern−Volmer constant for quenching of the unfolded protein by KI was increased 3.5-fold relative to that of the native receptor (Figure 3B). Both findings are consistent with increased solvent accessibility of RXRα tryptophan residues in the unfolded protein.

Stopped-flow experiments under pseudo-first-order conditions with a 9cRA concentration in excess over that of RXRα were fit to the single-exponential decay curve given in eq 3

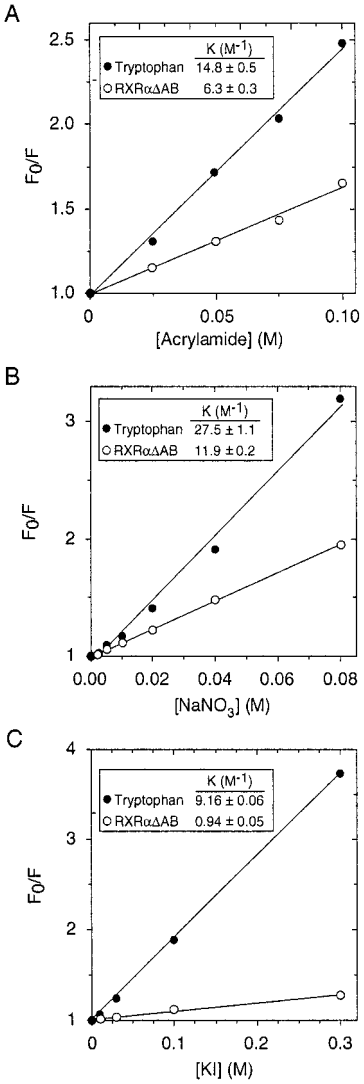

FIGURE 2: Stern−Volmer plots of collisional quenching experiments using wild-type mRXRα and acrylamide (A), $NaNO_3$ (B), and KI (C). Stern−Volmer constants (K) were obtained by fitting data to eq 1, giving the indicated values. Receptor and tryptophan concentrations were 1 μM. Shown are representative experiments that were replicated three to six times.

(Figure 4). To estimate the dissociation rate, a solution containing RXRα and 9cRA was mixed with an excess of a competitive ligand, SR11246 (*37*, *38*), that does not affect RXRα fluorescence emission (data not shown). The observed time-dependent fluorescence increase (Figure 5) was fit to eq 4, giving a value of 0.23 s^{-1} for the observed rate constant for 9cRA dissociation, k_2, at 25 °C. The plot of $1/\tau$ versus 9cRA concentration obtained at 9cRA concentrations of up to 3 μM was hyperbolic in shape (Figure 6). The simplest mechanism consistent with this concentration dependence is the two-step binding mechanism described by eq 5. The data were fit to eq 6 (Figure 6), giving a value for k_1 of 82 s^{-1} and a K of 2.34 μM at 25 °C. Calculation of the overall equilibrium constant, $K_{ov} = K(k_2/k_1)$, from the kinetic data gave a value of 6.4 nM which agreed quite well with the value determined from equilibrium binding data (7.6 nM; Figure 1).

The temperature dependence of k_2 was determined over the temperature range of 13−48 °C, and the values of k_1 and K were calculated from fits of the hyperbolic dependence of $1/\tau$ on 9cRA concentration to eq 6 at 13, 18, 25, and 30 °C (Table 1). Arrhenius and van't Hoff plots of the data are shown in Figure 7. From the Arrhenius plots, the activation energies (E_a) in the forward (k_1) and reverse (k_2) directions for the isomerization step were calculated from eq 7 to be 32 329 and 10 223 cal/mol, respectively, while $\Delta H°$ in the rapidly equilibrating binding reaction was calcluated to be equal to −17537 cal/mol from the fit of the temperature dependence of K to eq 8. From the value of E_a, $\Delta H°‡$, $\Delta S°‡$, and $\Delta G°‡$ for the isomerization step were calculated at 25 °C from eqs 9−11 (*40*):

Table 1: Temperature Dependence of Kinetic Constants

T (°C)	K^a (μM)	$k_1{}^a$ (s^{-1})	$k_2{}^b$ (s^{-1})
13	0.54 ± 0.07	8.02 ± 0.55	0.18 ± 0.01
18	0.65 ± 0.07	21.3 ± 1.2	0.25 ± 0.01
25	2.34 ± 0.46	82 ± 14	0.23 ± 0.01
30	2.11 ± 0.57	192 ± 104	0.50 ± 0.01

[a] Experimental values calculated from eq 5 where the value of k_2 was constrained to the experimentally determined value. [b] Determined from a fit of the data for SR11246 displacement of 9cRA to eq 4.

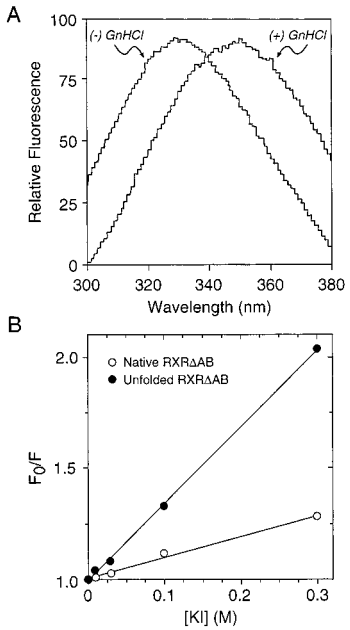

FIGURE 3: (A) Emission scans of wild-type mRXRα in the absence and presence of 6 M guanidine HCl. Note that the unfolded protein exhibits a fluorescence emission maximum near that of free tryptophan (357 nm) in contrast to that of the native protein (337 nm). (B) Stern−Volmer plot of KI quenching of native and unfolded mRXRα. The Stern−Volmer constants for native and unfolded receptor, determined as described in the legend of Figure 2, were 3.5 ± 0.1 and 0.94 ± 0.05 M^{-1}, respectively. Shown is a representative experiment that was replicated twice.

$$\Delta H°‡ = E_a - RT \tag{9}$$

$$\Delta S°‡ = R \ln\frac{kN_0\hbar}{RT} \tag{10}$$

$$\Delta G°‡ = \Delta H°‡ - T\Delta S°‡ \tag{11}$$

In eq 10, k is the value of the rate constant at 25 °C, N_0 is Avogadro's number, $\hbar$ is Planck's constant, and the value of the transmission coefficient is assumed to be 1. The values of K, k_1, and K_{ov} at 25 °C were then used in eq 12 to calculate $\Delta G°$ and $\Delta S°$ values at 25 °C, assuming that $\Delta H°$ is

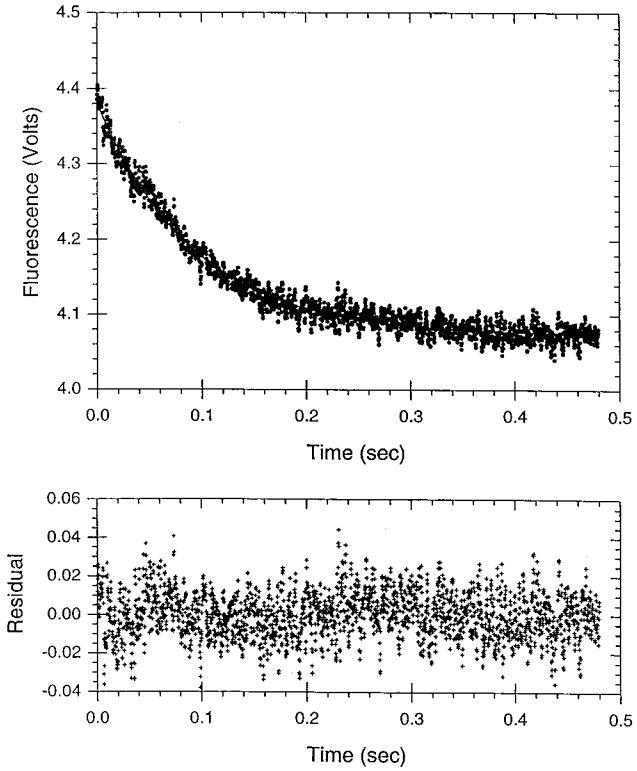

FIGURE 4: 9cRA binding to RXRα. Final concentrations of RXRα and 9cRA were 20 and 350 nM, respectively, and the experiment was carried out at 25 °C. The data were fit to eq 3, giving the following values: $A_1 = 4.073 \pm 0.001$ V, $A_2 = 0.308 \pm 0.001$ V, and $\tau^{-1} = 10.8 \pm 0.1$ s^{-1}; the theoretical line is based on these parameter estimates. The lower panel shows a plot of the residuals derived from this fit vs time.

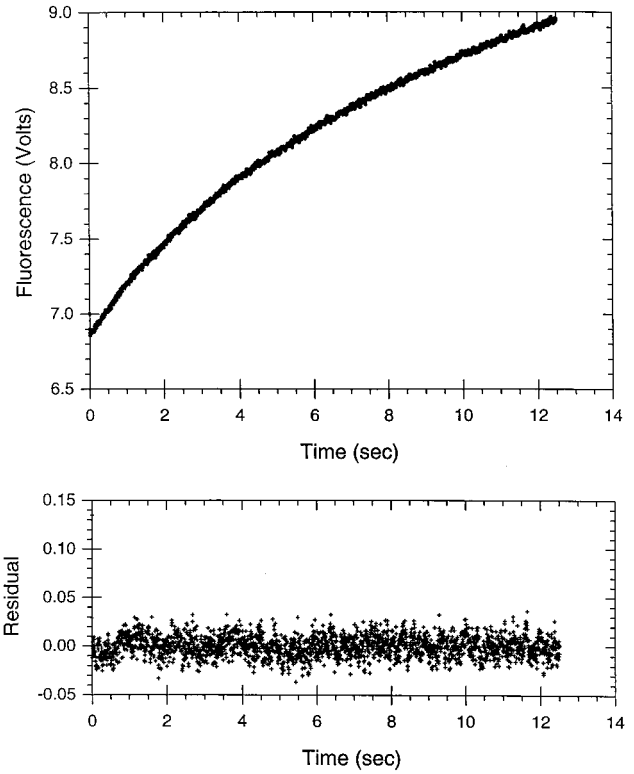

FIGURE 5: Displacement of 9cRA by SR11246 at 25 °C. 9cRA-liganded RXRα was mixed with SR11246, giving final concentrations of 50 nM and 1 μM, respectively. Data were fit to eq 4, giving the following values: $A_1 = 6.866 \pm 0.001$ V, $A_2 = 1.25 \pm 0.01$ V, $1/\tau = 0.225 \pm 0.002$ s^{-1}, and $k_2 = 0.073 \pm 0.001$ V/s. The line through the data represents the fitted curve, and the lower panel shows a plot of the corresponding residuals vs time.

temperature-independent from 18 to 30 °C, to map the free energy changes over the pathway of 9cRA binding to RXRα (Figure 8):

$$\Delta G^\circ = RT \ln K = \Delta H^\circ - T\Delta S^\circ \qquad (12)$$

Gel filtration chromatography and native gel electrophoresis experiments were carried out to determine the physical state of RXRα in the presence and absence of 9cRA toward the goal of identifying the species responsible for ligand-induced fluorescence quenching. Both types of analyses indicated that, in the absence of ligand, RXRα existed as a heterogeneous population of monomeric and tetrameric species (Figure 9A−C), in agreement with the data of Chen et al. (*35*). Gel filtration analysis (Figure 9A) suggested that approximately 20% of the RXRα population existed in the tetrameric form, whereas the fraction of tetrameric receptor as determined by native gel experiments was at least 50% (Figure 9C, lane 1). The basis for this descrepancy is unknown but may be related to the presence of 0.05% CHAPS in the gel filtration buffers, differential staining properties of monomeric and tetrameric forms of the receptor in acrylamide gels, or both. The presence of dimeric RXRα species could not be ruled out by gel filtration chromatography due to a lack of resolution (Figure 9A); however, a dimeric population of RXRα was undetectable in the native gel experiments performed in the absence of 9cRA (Figure 9C, lane 1). Addition of 9cRA converted all tetrameric species into RXRα monomers as revealed by both types of analyses (Figure 9B,C), consistent with the results of Chen et al. (*35*). Again, a dimeric form of RXRα was not detected in the presence of 9cRA in either gel filtration or native gel experiments (Figure 9B,C).

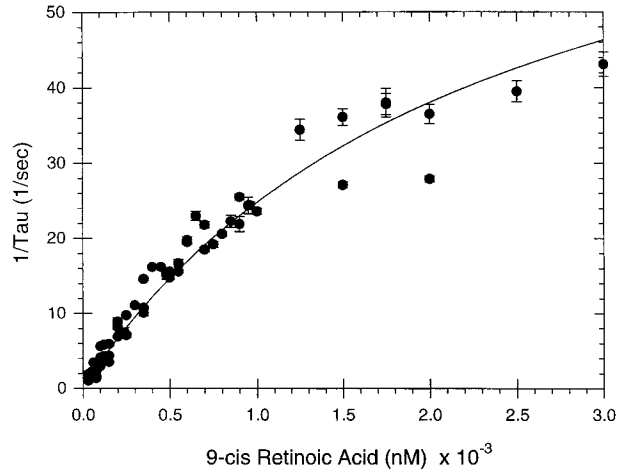

FIGURE 6: Dependence of $1/\tau$ on 9cRA concentration at 25 °C. Data from experiments in which 9cRA was in excess over RXRα were fit to eq 6 with k_2 fixed at 0.23 s^{-1} (see Figure 3), giving the following values: $k_1 = 82 \pm 14$ s^{-1} and $K = 2.34 \pm 0.46$ μM.

DISCUSSION

RXRα fluorescence emission arises from two tryptophan residues, Trp^{287} and Trp^{310}. The results of chemical quenching experiments presented herein suggest that one or both of these tryptophan residues may be buried within the hydrophobic core of the native protein and have limited solvent

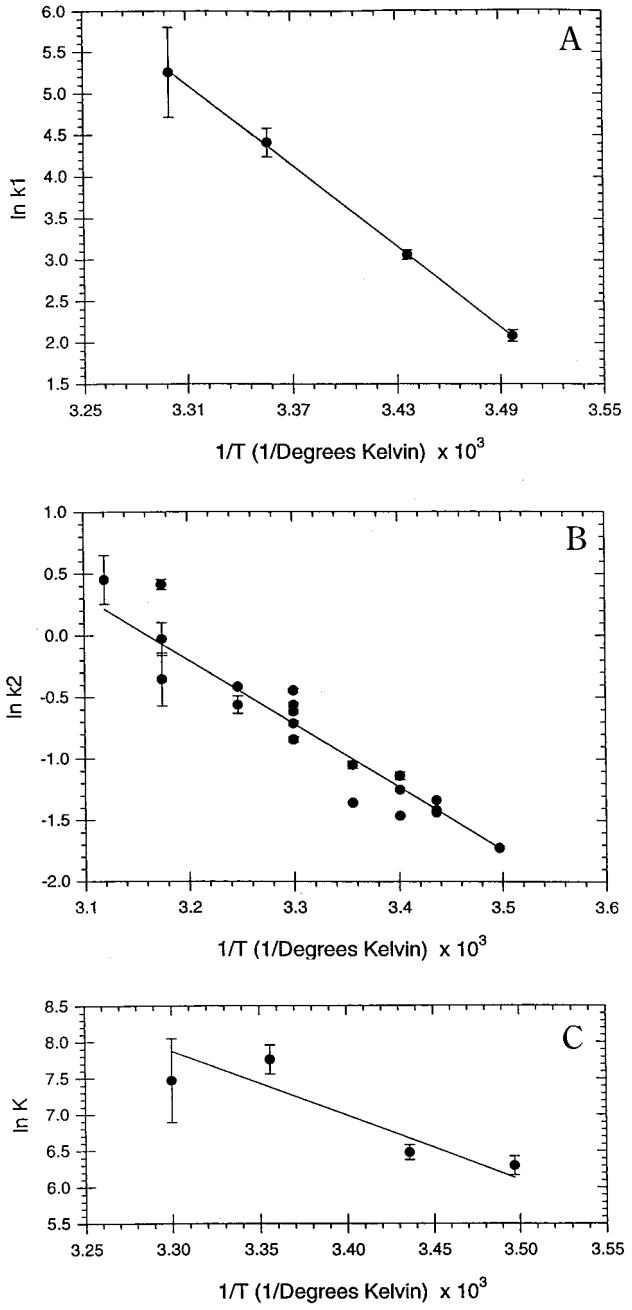

FIGURE 7: Temperature dependence of kinetic parameters. Arrhenius plots of k_1 (A) and k_2 (B) and a van't Hoff plot of K (C) vs $1/T$ were fit to either eq 7 (A and B) or eq 8 (C). Fitted values were as follows: for k_1, ln $A = 59.0 \pm 0.7$ and $E_a = 32.3 \pm 0.4$ kcal/mol; for k_2, ln $A = 16.3 \pm 1.7$ and $E_a = 10.2 \pm 1.0$ kcal/mol; and for K, $C = 37 \pm 11$ and $\Delta H° = -17.5 \pm 6.5$ kcal/mol.

accessibility. On the basis of the crystal structure of the ligand binding domain of human RXRα, Trp[287] and Trp[310] would be similarly positioned within α-helices 3 and 5, respectively (*25*−*27*), of the mouse RXRα protein used in these studies (*6*). Helices 3 and 5, together with residues from helices 1 and 11, loops 6−7 and 11−12, and the β-turn, are believed to form the lining of the RXRα ligand binding pocket (*25*−*27*). Thus, both Trp[287] and Trp[310] are well-positioned to function as "sensors" of ligand binding by RXRα. Because the dissociation constant we obtained for 9cRA binding to RXRα was nearly identical to that previously reported for [^{3}H]9cRA binding to this receptor (*3*, *41*), these fluorescence measurements appear to reflect the ligand binding activity of the receptor accurately. Previous [^{3}H]9cRA binding studies have typically employed gel filtration as a means of separating bound from free radioligand (*3*, *41*). As shown in Figure 5, the magnitude of the rate constant, k_2, for 9cRA dissociation from RXRα at 25 °C was determined to be 0.23 s^{-1}, which corresponds to a half-time of dissociation of approximately 3 s. Thus, the time required to accomplish the separation of bound from free radioligand by gel filtration would result in significant dissociation of bound [^{3}H]9cRA and an underestimation of the total amount of bound [^{3}H]-9cRA. In contrast, fluorescence quenching experiments do not involve perturbation of equilibrium conditions, thus facilitating a more accurate determination of the maximum binding capacity of the receptor and the affinity of RXRα for 9cRA. In agreement with previous studies (*21*, *22*), the stoichiometry of 9cRA binding to the multiple preparations of purified RXRα used in these studies was found to be 1:1, suggesting that the active fraction of receptors in these preparations approaches unity.

9cRA-mediated quenching of RXR intrinsic tryptophan fluorescence may result from the spectral overlap of tryptophan emission and 9cRA absorption, the corresponding maxima of which are 337 and 348 nm, respectively. Alternatively, 9cRA-mediated quenching of RXRα fluorescence may arise from ligand-induced alterations in the microenvironment surrounding one or both tryptophan residues. Such a ligand-induced RXRα conformational change is consistent with crystallographic data (*25*−*27*) and the results of differential proteolytic sensitivity assays (*14*, *20*). These two possibilities were distinguished by the high-affinity agonist SR11246, which displaces [^{3}H]9cRA from purified RXRα and promotes a receptor conformational change that appears to be identical to that induced by 9cRA as detected by differential proteolytic sensitivity assays (V. J. Peterson et al., unpublished data). However, SR11246 does not absorb light in the range of RXRα tryptophan emission (M. Leid et al., unpublished data), and thus, fluorescence quenching induced by this agonist could arise only from the induced RXRα conformational change. The maximal amplitude of fluorescence quenching induced by SR11246 is approximately $^1/_{10}$ of that induced by 9cRA (5 and 50%, respectively; Figure 1 and data not shown), suggesting that absorption of photons may represent the major mechanism by which 9cRA quenches the intrinsic tryptophan fluorescence of RXRα. If this is true, the conformational change that follows ligand binding must provide the correct orientation of 9cRA in the binding pocket and/or reduce the distance between the donor RXRα tryptophan residues and the acceptor 9cRA moiety such that fluorescence energy transfer can occur.

Ligand-induced conformational change may play multiple roles in the signaling pathways of nuclear receptors. Ligand binding has been shown to induce dissociation of receptor-associated heat shock proteins (*42*) and transcriptional corepressor proteins such as NCoR and SMRT (*17*). However, RXRα does not appear to associate significantly with any of the heat shock proteins or transcriptional corepressors that have been identified to date. Second, ligand-induced receptor conformational change appears to promote interaction of nuclear receptors with transcriptional coactivator proteins. Liganded RXRα has been shown to interact with TIF-1 (*43*), TIF-2 (*44*), SUG-1 (*45*), SRC-1 (*46*), and p300/

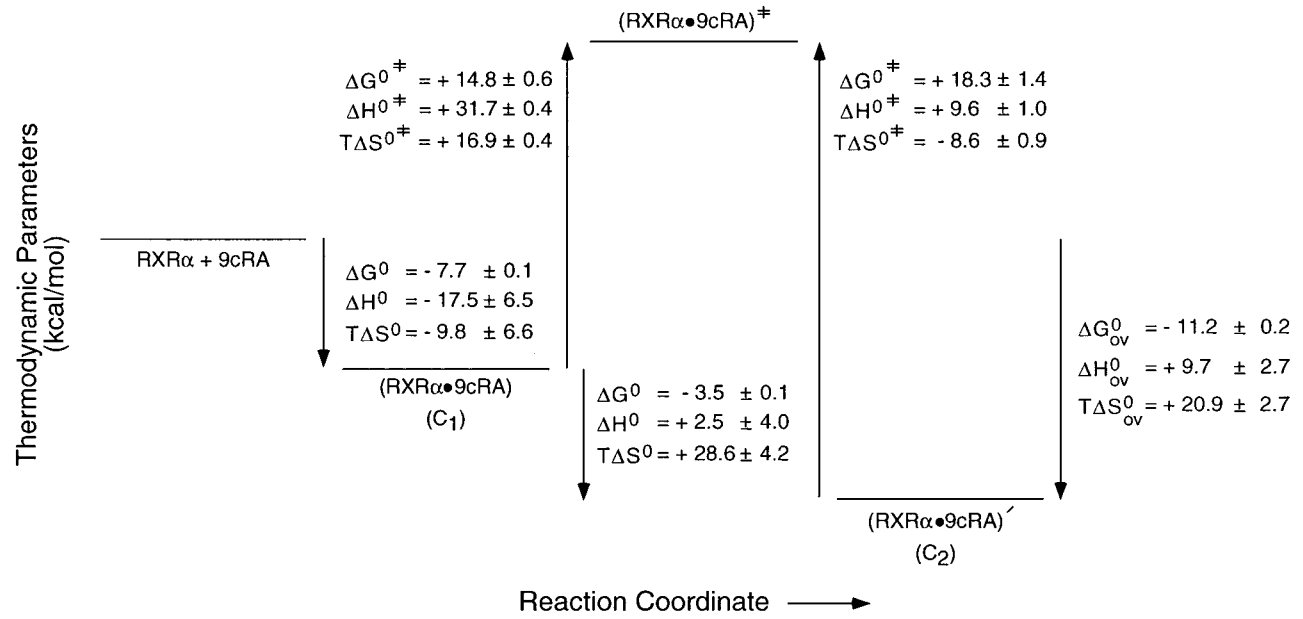

FIGURE 8: Reaction coordinate for 9cRA binding to RXRα at 25 °C. Data from the temperature dependence of the kinetic parameters were used to calculate $\Delta H^{\circ\ddagger}$, $\Delta S^{\circ\ddagger}$, and $\Delta G^{\circ\ddagger}$ for k_1 and k_2 (eqs 9−11) and ΔG° and ΔS° for K and K_{ov} (eq 12).

CBP (*47*). Thus, ligand-induced RXRα conformational change may serve as a molecular switch that promotes the formation of a receptor-containing, multiprotein complex that is competent to activate transcription of target genes. It is currently unknown if RXRα, like estrogen receptor α (*48*), can exist in two (or more) conformations that are stabilized by structurally distinct ligands. However, it is tempting to speculate that the differential activity of two RXR ligands, LGD10268 and LGD10754 (*16*), may arise from induction and/or stabilization of different conformations of the receptor. In this respect, it will be of interest to determine if these two ligands differentially quench the intrinsic tryptophan fluorescence of RXRα in transient kinetic studies. Finally, binding of 9cRA by RXRα has been demonstrated to modulate the oligomeric state of the protein in solution and on DNA response elements (*35*, *49*−*51*), suggesting another possible role of ligand-induced RXRα conformational change.

The simplest kinetic mechanism consistent with the hyperbolic dependence of $1/\tau$ on 9cRA concentration under conditions where [9cRA] ≫ [RXRα] is given by eq 4. The mechanism consists of two steps: a binding step which equilibrates rapidly (K) followed by a slow conformational change (k_1 and k_2). The change in fluorescence intensity is attributed to the formation of the final complex, C_2, in the slow step. Such a mechanism would be consistent with the electrostatic field guidance model proposed by Moras and colleagues (*25*) in which *trans*-RA is directed to the ligand binding pocket of hRARγ by ionic interactions between the carboxylate group of the ligand and basic amino acids at the entrance of the cavity. The ligand is then tunneled toward the hydrophobic ligand binding cavity by electrostatic attraction between both R^{278} and K^{236} and the carboxylate group of *trans*-RA which serves to anchor the ligand in the binding pocket (*25*).

Control experiments in which a change in fluorescence was observed after SR11246 was mixed with buffer showed a slow increase in fluorescence with an observed rate equal to that found for the steady state component (k_2) in the 9cRA dissociation experiments. Therefore, the SR11246 competition data (Figure 5) were fit to eq 3 to obtain a value for k_2. This value was then constrained to calculate k_1 and K from the dependence of $1/\tau$ on [9cRA] from eq 6 (Figure 6). For the mechanism described in eq 4, the fractional saturation, $\bar{Y}$, is given by

$$\bar{Y} = \frac{l}{l + \dfrac{KK_1}{1 + K_1}} = \frac{l}{l + K_{ov}} \qquad (13)$$

From the kinetic data, it can be seen that $k_2/k_1 = K_1 \ll 1$, and the value for the overall dissociation constant, K_{ov}, equals KK_1. The value of K_{ov} from the fit to the kinetic data (6.4 nM) was in excellent agreement with that found from the equilibrium fluorescence titrations (7.6 nM), an indication of the consistency between the two methods.

Two mechanisms that are not compatible with the hyperbolic dependence of $1/\tau$ on [9cRA] are (1) a simple biomolecular association mechanism that predicts a linear dependence of $1/\tau$ on [9cRA] and (2) the case where a slow protein isomerization step precedes rapid ligand binding which predicts that $1/\tau$ should decrease as [9cRA] increases (*52*). The possibility of a kinetic mechanism involving subunit association and dissociation steps was also considered. Because most of these mechanisms do not exhibit exponential behavior or are not analytically solvable, a complete analysis was not feasible. However, two experimental observations were made. First, under psuedo-first-order conditions ([9cRA] = 1 μM), varying the concentration of RXRα from 25 to 100 nM had no effect on the observed value of $1/\tau$. Second, when the dissociation rate of 9cRA was measured (final concentrations for SR11246 and 9cRA of 1 μM and 100 nM, respectively) at RXRα concentrations ranging from 40 nM to 1 μM, no effect of varying protein concentration was observed. These observations are most easily reconciled with a mechanism in which subunit association or dissociation is not required or at least not rate-limiting. It was possible to analyze a simplified mechanism

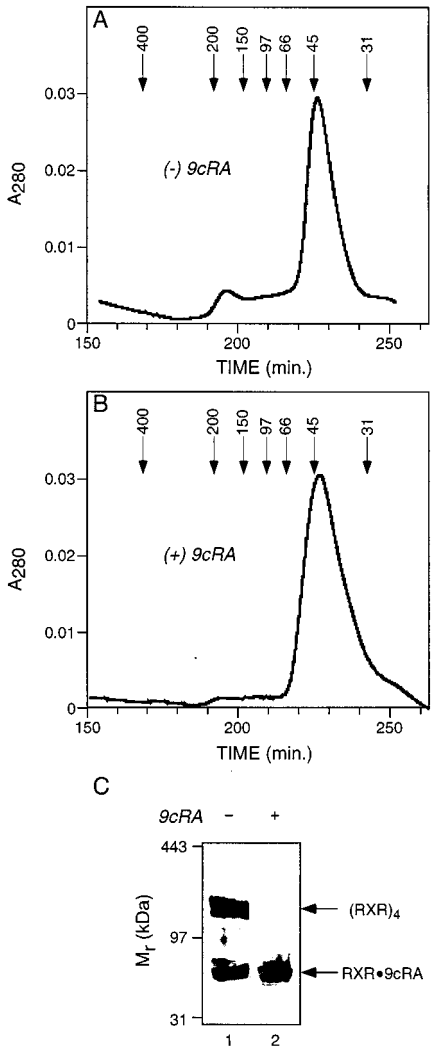

FIGURE 9: Gel filtration analysis of RXRα in the absence (A) and presence (B) of 5 μM 9cRA. Purified RXRα (500 μL, 4.2 μM in TDN buffer) was incubated with vehicle (0.5% v/v ethanol, A) or 9cRA (final concentration of 5 μM, B) for 60 min on ice and then chromatographed as described in Experimental Procedures. The elution positions of molecular mass standards (determined prior to and following RXRα chromatography in the absence and presence of 9cRA) are denoted by downward arrows. (*C*) Native gel analysis of RXRα in the absence (lane 1) and presence (lane 2) of 5 μM 9cRA. Lanes 1 and 2, which were derived from two different gels, were aligned by the migration of the indicated marker proteins. Protein bands corresponding to a RXRα tetramer and a liganded RXRα monomer are denoted by arrows.

in which subunit dissociation from tetramer (R_4) to dimer (R_2) to monomer is assumed to be irreversible:

$$4l + R_4 \xrightarrow{k_a} 4l + R_2 \xrightarrow{k_b} 4R + 4l + R_4 + 4l \overset{K}{\rightleftharpoons} 4C_1 \underset{k_{-1}}{\overset{k_1}{\rightleftharpoons}} 4C_2 \quad (14)$$

If it is assumed that the fluorescence change is due to C_2 formation, the above model predicts a three-exponential equation:

$$C_2 = k_1'R_0[p - qe^{-k_a t} + re^{-k_b t} + se^{-(k_1'+k_2)t}] \quad (15)$$

where $k_1' = k_1 l_0/(K + l_0)$, $p = (k_1' + k_2)^{-1}$, $q = (k_1' + k_2 - k_a)^{-1} + r$, $r = k_a/(k_b - k_a)$, and $s = q - r - p$. Under conditions when $k_b \gg k_a \gg (k_1' + k_2) \geq 1$, $q = r = 0$ and eq 15 reduces to

$$C_2 = \frac{k_1'R_0}{k_1' + k_2}[1 - e^{(k_1'+k_2)t}] \quad (16)$$

giving rise to the same kinetic behavior as eq 5. If it is assumed that analysis of transition state thermodynamic parameters by Arrhenius plots can be applied in this system, the temperature dependence of kinetic paramters K, k_1, and k_2 and the calculated values for K_1 ($=k_2/k_1$) and K_{ov} ($=KK_1$) were used to propose a reaction coordinate diagram for the binding of 9cRA to RXRα at 25 °C (Figure 8). The association step to form C_1 from free RXRα and 9cRA is driven by a favorable enthalpy change which is used to overcome an unfavorable entropic contribution to binding due, at least in part, to reducing the degrees of freedom of the system. The isomerization step from C_1 to C_2 is enthalpically unfavorable, but the dominant entropy term results in a negative value of ΔG for this step of the reaction as well. Such a large entropy change might result from loss of protein-associated water molecules occurring in conjunction with a rearrangement of the tertiary structure of the protein. The overall reaction is enthalpically unfavorable and is driven to the right by the large and favorable entropy change caused by the C_1 to C_2 isomerization step. This observation would be consistent with the notion that because RXRα may associate with either itself or other RXR subtypes, numerous heterodimerization partners, transcriptional coactivators, scaffolding proteins, and DNA response elements, it is a conformationally flexible molecule and ligand binding most likely causes large structural rearrangements reflected in the entropic component of the overall binding mechanism.

ACKNOWLEDGMENT

We thank P. Chambon and P. Kastner for the parental mouse RXRα expression vector from which RXRαΔAB-His was derived, and we gratefully acknowledge the assistance of the Nucleic Acid and Protein Core Facility of the Oregon State University Environmental Health Sciences Center.

REFERENCES

1. Chambon, P. (1996) *FASEB J. 10*, 940−54.
2. Kastner, P., Mark, M., and Chambon, P. (1995) *Cell 83*, 859−69.
3. Levin, A. A., Sturzenbecker, L. J., Kazmer, S., Bosakowski, T., Huselton, C., Allenby, G., Speck, J., Kratzeisen, C., Rosenberger, M., Lovey, A., et al. (1992) *Nature 355*, 359−61.
4. Heyman, R. A., Mangelsdorf, D. J., Dyck, J. A., Stein, R. B., Eichele, G., Evans, R. M., and Thaller, C. (1992) *Cell 68*, 397−406.
5. Yu, V. C., Delsert, C., Andersen, B., Holloway, J. M., Devary, O. V., Naar, A. M., Kim, S. Y., Boutin, J. M., Glass, C. K., and Rosenfeld, M. G. (1991) *Cell 67*, 1251−66.
6. Leid, M., Kastner, P., Lyons, R., Nakshatri, H., Saunders, M., Zacharewski, T., Chen, J. Y., Staub, A., Garnier, J. M., Mader, S., et al. (1992) *Cell 68*, 377−95.
7. Kastner, P., Mark, M., Leid, M., Gansmuller, A., Chin, W., Grondona, J. M., Decimo, D., Krezel, W., Dierich, A., and Chambon, P. (1996) *Genes Dev. 10*, 80−92.
8. Leid, M., Kastner, P., and Chambon, P. (1992) *Trends Biochem. Sci. 17*, 427−33.

9. Zechel, C., Shen, X. Q., Chen, J. Y., Chen, Z. P., Chambon, P., and Gronemeyer, H. (1994) *EMBO J. 13*, 1425−33.
10. Kurokawa, R., DiRenzo, J., Boehm, M., Sugarman, J., Gloss, B., Rosenfeld, M. G., Heyman, R. A., and Glass, C. K. (1994) *Nature 371*, 528−31.
11. Kurokawa, R., Soderstrom, M., Horlein, A., Halachmi, S., Brown, M., Rosenfeld, M. G., and Glass, C. K. (1995) *Nature 377*, 451−4.
12. Forman, B. M., Umesono, K., Chen, J., and Evans, R. M. (1995) *Cell 81*, 541−50.
13. Kersten, S., Dawson, M. I., Lewis, B. A., and Noy, N. (1996) *Biochemistry 35*, 3816−24.
14. Minucci, S., Leid, M., Toyama, R., Saint-Jeannet, J. P., Peterson, V. J., Horn, V., Ishmael, J. E., Bhattacharyya, N., Dey, A., Dawid, I. B., and Ozato, K. (1997) *Mol. Cell Biol. 17*, 644−55.
15. Chen, J. Y., Clifford, J., Zusi, C., Starrett, J., Tortolani, D., Ostrowski, J., Reczek, P. R., Chambon, P., and Gronemeyer, H. (1996) *Nature 382*, 819−22.
16. Lala, D. S., Mukherjee, R., Schulman, I. G., Koch, S. S., Dardashti, L. J., Nadzan, A. M., Croston, G. E., Evans, R. M., and Heyman, R. A. (1996) *Nature 383*, 450−3.
17. Torchia, J., Glass, C., and Rosenfeld, M. G. (1998) *Curr. Opin. Cell Biol. 10*, 373−83.
18. Moras, D., and Gronemeyer, H. (1998) *Curr. Opin. Cell Biol. 10*, 384−91.
19. Allan, G. F., Leng, X., Tsai, S. Y., Weigel, N. L., Edwards, D. P., Tsai, M. J., and O'Malley, B. W. (1992) *J. Biol. Chem. 267*, 19513−20.
20. Leid, M. (1994) *J. Biol. Chem. 269*, 14175−81.
21. Chen, Z. P., Shemshedini, L., Durand, B., Noy, N., Chambon, P., and Gronemeyer, H. (1994) *J. Biol. Chem. 269*, 25770−6.
22. Cheng, L., Norris, A. W., Tate, B. F., Rosenberger, M., Grippo, J. F., and Li, E. (1994) *J. Biol. Chem. 269*, 18662−7.
23. Kersten, S., Pan, L., Chambon, P., Gronemeyer, H., and Noy, N. (1995) *Biochemistry 34*, 13717−21.
24. Kersten, S., Kelleher, D., Chambon, P., Gronemeyer, H., and Noy, N. (1995) *Proc. Natl. Acad. Sci. U.S.A. 92*, 8645−9.
25. Renaud, J. P., Rochel, N., Ruff, M., Vivat, V., Chambon, P., Gronemeyer, H., and Moras, D. (1995) *Nature 378*, 681−9.
26. Bourguet, W., Ruff, M., Chambon, P., Gronemeyer, H., and Moras, D. (1995) *Nature 375*, 377−82.
27. Wurtz, J. M., Bourguet, W., Renaud, J. P., Vivat, V., Chambon, P., Moras, D., and Gronemeyer, H. (1996) *Nat. Struct. Biol. 3*, 87−94.
28. Klaholz, B. P., Renaud, J. P., Mitschler, A., Zusi, C., Chambon, P., Gronemeyer, H., and Moras, D. (1998) *Nat. Struct. Biol. 5*, 199−202.
29. Le Douarin, B., Nielsen, A. L., Garnier, J. M., Ichinose, H., Jeanmougin, F., Losson, R., and Chambon, P. (1996) *EMBO J. 15*, 6701−15.
30. Heery, D. M., Kalkhoven, E., Hoare, S., and Parker, M. G. (1997) *Nature 387*, 733−6.
31. Torchia, J., Rose, D. W., Inostroza, J., Kamei, Y., Westin, S., Glass, C. K., and Rosenfeld, M. G. (1997) *Nature 387*, 677−84.
32. McInerney, E. M., Rose, D. W., Flynn, S. E., Westin, S., Mullen, T. M., Krones, A., Inostroza, J., Torchia, J., Nolte, R. T., Assa-Munt, N., Milburn, M. V., Glass, C. K., and Rosenfeld, M. G. (1998) *Genes Dev. 12*, 3357−68.
33. Westin, S., Kurokawa, R., Nolte, R. T., Wisely, G. B., McInerney, E. M., Rose, D. W., Milburn, M. V., Rosenfeld, M. G., and Glass, C. K. (1998) *Nature 395*, 199−202.
34. Darimont, B. D., Wagner, R. L., Apriletti, J. W., Stallcup, M. R., Kushner, P. J., Baxter, J. D., Fletterick, R. J., and Yamamoto, K. R. (1998) *Genes Dev. 12*, 3343−56.
35. Chen, Z., Iyer, J., Bourguet, W., Held, P., Mioskowski, C., Lebeau, L., Noy, N., Chambon, P., and Gronemeyer, H. (1998) *J. Mol. Biol. 275*, 55−65.
36. Lakowicz, J. R. (1983) *Principles of Fluorescence Spectroscopy*, Plenum, New York.
37. Kizaki, M., Dawson, M. I., Heyman, R., Elster, E., Morosetti, R., Pakkala, S., Chen, D. L., Ueno, H., Chao, W., Morikawa, M., Ikeda, Y., Heber, D., Pfahl, M., and Koeffler, H. P. (1996) *Blood 87*, 1977−84.
38. de Vos, S., Dawson, M. I., Holden, S., Le, T., Wang, A., Cho, S. K., Chen, D. L., and Koeffler, H. P. (1997) *Prostate 32*, 115−21.
39. Bevington, P. R. (1969) *Data Reduction and Error Analysis for the Physical Sciences*, McGraw-Hill, New York.
40. Daniels, F., and Alberty, R. A. (1966) *Physical Chemistry*, 3rd ed., Wiley, New York.
41. Allenby, G., Janocha, R., Kazmer, S., Speck, J., Grippo, J. F., and Levin, A. A. (1994) *J. Biol. Chem. 269*, 16689−95.
42. Tsai, M. J., and O'Malley, B. W. (1994) *Annu. Rev. Biochem. 63*, 451−86.
43. LeDouarin, B., Zechel, C., Garnier, J. M., Lutz, Y., Tora, L., Pierrat, P., Heery, D., Gronemeyer, H., Chambon, P., and Losson, R. (1995) *EMBO J. 14*, 2020−33.
44. Voegel, J. J., Heine, M. J., Zechel, C., Chambon, P., and Gronemeyer, H. (1996) *EMBO J. 15*, 3667−75.
45. vom Baur, E., Zechel, C., Heery, D., Heine, M. J., Garnier, J. M., Vivat, V., Le Douarin, B., Gronemeyer, H., Chambon, P., and Losson, R. (1996) *EMBO J. 15*, 110−24.
46. Dowell, P., Ishmael, J. E., Avram, D., Peterson, V. J., Nevrivy, D. J., and Leid, M. (1997) *J. Biol. Chem. 272*, 33435−43.
47. Kamei, Y., Xu, L., Heinzel, T., Torchia, J., Kurokawa, R., Gloss, B., Lin, S. C., Heyman, R. A., Rose, D. W., Glass, C. K., and Rosenfeld, M. G. (1996) *Cell 85*, 403−14.
48. Brzozowski, A. M., Pike, A. C., Dauter, Z., Hubbard, R. E., Bonn, T., Engstrom, O., Ohman, L., Greene, G. L., Gustafsson, J. A., and Carlquist, M. (1997) *Nature 389*, 753−8.
49. Kersten, S., Pan, L., and Noy, N. (1995) *Biochemistry 34*, 14263−9.
50. Kersten, S., Gronemeyer, H., and Noy, N. (1997) *J. Biol. Chem. 272*, 12771−7.
51. Dong, D., and Noy, N. (1998) *Biochemistry 37*, 10691−700.
52. Gutfreund, H. (1995) *Kinetics for the Life Sciences*, Cambridge University Press, New York.

BI9829478